Condensation heat transfer of CO_2 on Cu based hierarchical and nanostructured surfaces

Ingrid Snustad [a],*, Lene Hollund [a], Åsmund Ervik [b], Anders Austegard [b], Amy Brunsvold [b], Jianying He [a], Zhiliang Zhang [a]

[a] Faculty of Engineering, Department of Structural Engineering, Norwegian University of Science and Technology, Richard Birkelands vei 1A, Trondheim 7491, Norway
[b] SINTEF Energy Research, Sem Sæ lands vei 11, Trondheim 7034, Norway

A B S T R A C T

Phase-change processes such as condensation are efficient means of heat transfer. However, condensation is also an energy-intensive process and extensive research is conducted to increase the heat transfer efficiency. Increasing the effective heat transfer area in terms of surface structures on macro or microscale is one such technique of heat transfer enhancement. In this work, we have studied micro- and nanostructured surfaces for their potentials in increasing heat transfer during condensation of CO_2. Three Cu-based surfaces on which CuO nanoneedles have been grown, have been investigated. We hypothesize three competing mechanisms govern the overall heat transfer on structured surfaces: (1) increased heat transfer area, (2) lower thermal conductivity of oxides, and (3) condensate flooding of the structures. Our study has shown that in some cases, the effect of these mechanisms can be neutralized. More importantly, the results show that superior heat transfer can be achieved by optimizing the surface structure. The best of the structured surfaces resulted in a heat transfer coefficient 66% higher than that of the unstructured surface.

1. Introduction

Condensation heat transfer performance influences several industrial processes and is especially important for heat exchanger technology. CO_2 is identified as an alternative for reducing the usage of fluorine based refrigerants in heat exchangers and heat pumps due to their negative environmental impact [1–3]. CO_2 has a high triple point and low critical point, and has therefore the potential to be an efficient refrigerant [4]. Increased condensation heat transfer efficiency will reduce the energy consumption of the liquefaction process and reduce the costs of heat exchangers and heat pumps. Liquefaction of CO_2 is also a part of Carbon Capture and Storage (CCS), especially as a preprocess for ship transport [5,6]. Increased liquefaction efficiency will reduce the energy consumption and the cost of the CCS systems, which is necessary to scale up the number of CCS projects worldwide [7].

In the literature, there are several examples of studies on the increase of heat transfer efficiency by the use of micro- and nanos-

tructures on the surface [8,9]. Hendricks et al. [10] fabricated ZnO flower-like nanostructures on Al and Cu and reported increased critical heat flux (CHF) for both surfaces. An increased CHF is related to a higher possible operational limit, and therefore a better heat transfer performance. The same phenomenon is reported by Nam et al. [11] and by Saedi and Alemrajabi [12]. The first reported an increase in CHF at wicking structures of CuO nanostructures on top of Cu microposts and the latter reported an increase in both CHF and heat transfer coefficient (HTC) on anodized Al surfaces. In pool boiling, an increased number of nucleation sites on the structured surfaces has proven beneficial for heat transfer. For example Li et al. [13] studied nucleation boiling on Cu nanorods deposited on a Cu surface, and found that there were 30 times as many bubble nucleation sites on the structured surfaces. They also found that the nanorod surface exhibited a higher wettability towards water, which reduced the size of the bubble diameter and increases the release frequency of the bubbles. By these mechanisms the CHF, and hence the heat transfer efficiency, was increased. Chen et al. [14] reported an increased HTC for pool boiling on nanowires of both Cu and Si. The improved HTCs were caused by the increased number of bubble nucleation sites in the microscale cavities in between the nanowires. The boiling curves

---

measured on both Cu and Si nanowires are similar to each other even though the thermal conductivity of the two materials are very different. The above results indicate that the heat transfer is dominated by the nucleation and bubble dynamics, not by the heat conduction, and the surface morphology is the determining factor.

For condensation, the number of nucleation sites have also been shown to increase on nanostructured surfaces. In the work by Boreyko and Chen, a hierarchical surface of Si micropillars covered with carbon nanotubes was investigated and the nucleation sites increased significantly along with a decrease in wettability [15]. The fabrication of the micro- and nanostructures resulted in a superhydrophobic surface on which the condensation occurred in the dropwise mode. Dropwise condensation results in HTCs up to an order of magnitude higher than the conventional filmwise condensation. On the surface by Boreyko et al., the droplets spontaneously jumped off at a droplet size much smaller than for a hydrophobic surface where the droplets are removed by gravity. On the other hand, not all superhydrophobic surfaces promotes dropwise condensation, but could actually cause a degradation of heat transfer [16]. The surface structures could in this case be flooded by the condensate, which is then strongly pinned to the surface even though the applied models predict that the surface is non-wetting. Dropwise condensation is a dynamic process and the droplets can nucleate and grow in between the structures, and consequently, be pinned to a superhydrophobic surface [8]. For this reason, superhydrophobic surfaces do not necessarily promote dropwise condensation.

Both the above mentioned studies, and others examining micro- and nanostructures for enhanced condensation heat transfer [17,18], have explored the beneficial performance of dropwise condensation. For low surface tension fluids, however, it is extremely challenging to obtain dropwise condensation as most condensates will flood the nanostructures. Aili et al. [19] studied the filmwise condensation heat transfer of a low surface tension fluid on microstructures on aluminium. They found that the heat transfer was unaffected by the microstructures. They also studied how nanostructures on a mini-fin Cu surface influenced the heat transfer performance. In this case, the heat transfer was reduced on the nanostructured surface due to solid-liquid friction, which results in a thicker condensate film on the surface. The heat transfer on a pure mini-fin Cu surface was, however, higher than on an unstructured surface, showing that increasing the effective condensation area was beneficial. The increase in heat transfer due to augmented surfaces is well-established and models describing the effect of different augmentation geometries have been developed by Ali [20] and Ali and Briggs [21]. The models include geometrical parameters in addition to the effect of the ratio between surface tension and gravity. The latter has a large impact on the flooding of the surface structures, revealing that a low surface tension fluid is less likely to flood the structures. For such fluids, a surface augmentation with small pitches between the structures would be more beneficial than for a high surface tension fluid, such as water.

Even though there are examples of studies on dropwise condensation of low surface tension fluids, no such studies exist for CO_2. Even though the refrigerant R134-a has proven to have similar flow behavior to CO_2 [22], the specific heat transfer behavior of filmwise CO_2 condensation is lacking. In previous work, using molecular dynamics simulations, we have investigated the condensation mechanism of CO_2 on Cu like surfaces [23,24]. Still, experimental studies have not yet been published for condensation of CO_2 on structured surfaces. To address this, we have in this work investigated CO_2 condensation on one untreated Cu surface and three micro- and nanostructured Cu based surfaces. The untreated surface serves as the baseline for the comparison of the heat transfer behavior of the modified surfaces. Of those, two are hierarchical in scale, with an underlying microstructure covered with nanos-

tructures. The third substrate is purely nanostructured, with randomly oriented nanoneedles covering the entire surface. The heat transfer performance of the four substrates are evaluated and compared. The aim of the study is to determine if and how micro- and nanostructures influence the heat transfer during filmwise condensation of a low surface tension fluid.

The main findings of the work is that the heat transfer is determined by the competing effect of nanostructures and the reduced thermal conductivity of CuO. The nanostructures induces a wicking condensation mode, which increases the heat transfer compared to filmwise mode, but the reduced thermal conductivity of CuO reduces the potential heat transfer increase and the heat transfer is therefore unaltered when the nanostructure density is high.

This paper is organized as follows. First, we describe the experimental method applied for measuring the condensation heat transfer followed by details on the fabrication of the three structured surfaces. Second, the results are presented along with a discussion of their meaning and significance. Finally, conclusions are drawn and some further work is stipulated. The results of a study of the mechanical durability of the nanostructures as a response to CO_2 condensation is included in the Supplementary Information.

2. Method and materials

The experimental method used for measuring heat flux and HTCs in this work is described in detail in our previous work [25]. A summary of the method and a description of the fabrication methods for the hierarchical and nanostructured surfaces are given in this section.

2.1. Experimental method

The experimental method relies on one dimensional heat transport through an insulated Cu cylinder, where a cooling element is attached to one end, and the investigated surface to the other. Four type K thermocouples (Omega Engineering) are embedded in the center of the cylinder to obtain the axial temperature gradient in the cylinder, which in turn is used to calculate the heat flux. The uncertainty of the thermocouples provided by the manufacturer is 1 K. To reduce the uncertainty, the thermocouples are cold junction compensated in a water cooling bath (Julabo) and calibrated on site in an ice bath. By this procedure the uncertainty is reduced and taken to be equal to the standard deviation of the measurements in the ice bath calibration, which was 0.02 K.

The cooling element attached to the Cu cylinder is a Cu block with narrow channels. Within the channels, two phase CO_2 is flowed through and evaporated, with a back-pressure regulator ensuring that the pressure inside the cooling element is the saturation pressure for the desired temperature. In this way, the CO_2 is kept at the boiling curve and two phase flow is kept throughout the cooling element. The temperature on the surface of the cooling element is thus uniform and accurately controlled by a back pressure regulator (Alicat PC3). The available temperature range is 55 to 20 °C, corresponding to a saturation pressure from 5.7 to 19.7 bar.

The investigated substrate is attached to the Cu cylinder with a thermal interface material (TIM (Aldrich Chemistry, Silver conductive paste, 735825-25G)). Prior to attachment, the baseline Cu surface is cleaned with acetone, isopropanol and ethanol (VWR, 99% reagent grade), in that order. The structured surfaces were cleaned prior to structure fabrication and kept in closed compartments to avoid deterioration of the micro- and nanostructures prior to heat transfer experiments.

The cooling element with the attached cylinder and substrates are placed in a pressure chamber consisting of a steel pipe closed off by flanges and bolts. A sight glass is embedded in one flange
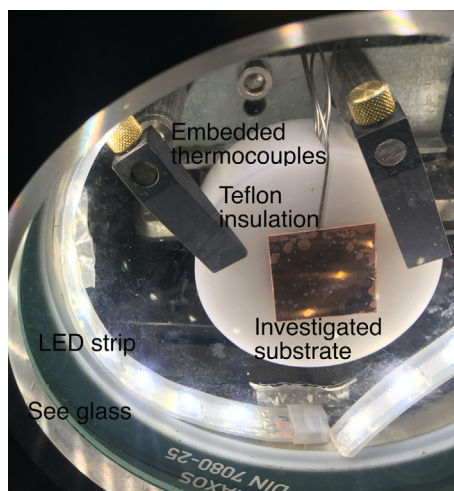
Fig. 1. Photograph of the investigated substrate as seen through the glass in the end flange of the pressure chamber. The embedded thermocouples are also seen. The Cu cylinder is enclosed in the teflon insulation and is hidden behind the substrate. A LED strip enlightening the substrate is also shown.

and a high speed camera (Phantom 9.1) is placed close to the glass for in situ observation of the condensation process. Specifically, the onset of the condensation is observed. The pressure chamber is built for pressures up to 20 bar and is filled by pure CO_2 (5.2, AGA Scientific Grade) during experiments. A pressure regulator (Alicat PCD) maintains a constant pressure in the chamber, also during condensation. The end flange with the see glass and the substrate within the chamber is shown in Fig. 1.

The temperature in the Cu cylinder is controlled, monitored and acquired with a LabView™ interface. In addition, the pressure in the chamber, the temperature of the gas and in the cooling element is controlled and monitored by the software.

2.2. Material fabrication and surface description

Four substrates have been investigated in this work: (a) an untreated Cu plate, (b) a nanostructured Cu surface, (c) and (d) micro- and nanostructured surfaces with variation in nanostructure density. All substrates were initially 0.5 mm thick quadratic (2.5 × 2.5 cm) Cu plates (99.9% purity, Sigma-Aldrich). The baseline Cu is untreated and has a low intrinsic roughness. The root mean square (RMS) roughness is measured in a Veelco Dektak 150 profilometer to be 73 nm.

The nanostructured surface is fabricated with an adaption of the solution immersion technique developed by He et al. [26,27]. The Cu substrate is cleaned with acetone and isopropanol, dried with nitrogen and immersed into a solution of 0.1 M ammonium persulfate and 2.5 M sodium hydroxide for 3 M. The surface is then dried at 120 °C to fully dehydrate the structures, resulting in a surface with stable CuO nanoneedles, see Fig. 2. The width of the nanoneedles is on average 175 nm and the average length is 3 μm. The nanoneedles initially grow at nucleation sites with high surface energy such as spikes and hills on the surface. Therefore, the underlying surface structure of the Cu surface is observed as lines with higher nanoneedle density. The nanostructured surface is henceforth named NS. Note here that the nanoneedles are made of the oxide corresponding to the substrate metal, i.e. CuO, a point which will prove to be important for the subsequent condensation heat transfer analysis.

For fabricating the hierarchical structures, the first step is to etch micropillars into the Cu substrate by photolithography and chemical assisted ion beam etch (CAIBE). Photolithography is a process for transferring a pattern onto a surface by exposing the

surface covered in a photoreactive material (photoresist) with a laser in a predefined pattern. The photoresist hardens and works as a mask for the following etching process. CAIBE is an etching method for physical sputtering of unprotected material on a surface. In this work, photoresist micropillars with a diameter of 10 μm were deposited onto the Cu surface. These micropillars protected the underlying Cu in the CAIBE process, and the material around the photoresist was etched. The resulting surface pattern after photolithgraphy and CAIBE are Cu micropillars, shown in Fig. 3. The micropillars are on average 10 μm in diameter and 1 μm in height. For the two hierarchical surfaces, the exposure doses in the photolithography process were the only fabrication difference. One surface, Fig. 3(a), was exposed with a laser with 1700 mJ cm^{-2} energy flux, and the other, Fig. 3(b) was exposed with 1900 mJ cm^{-2} energy flux. This difference affect the resulting nanostructure density as described below.

Following the micropillar fabrication, the nanostructures on top of the microstructures are fabricated in the solution immersion process described above, with an immersion time of 5 M. The resulting nanoneedles are approximately 10 μm long for both surfaces. The morphology is different on the surface exposed with 1700 mJ cm^{-2} and the one exposed with 1900 mJ cm^{-2}. Henceforth the first is called S17 and the latter is called S19. The two surfaces are shown in Figs. 4 and 5, respectively. It is observed that the nanoneedles grow more uniformly on the S19 surface compared to the S17 surface. On the S17 surface, there is a large variation in the nanoneedle density across the surface and the nanoneedles grow both on the sides and on top of the micropillars. However, the nanoneedles grown on the top of the micropillars are shorter. Around the majority of the micropillars the nanoneedles have grown in the horizontal direction, normal to the micropillar circumference. At the rest of the micropillars the nanoneedles have grown in all directions causing dense clusters on the sides and top of the micropillars. On the S19 surface, the nanoneedles grow, to a large degree, only on the sides of the micropillars and with a more uniform and higher density than on S17. On the S17 surface clusters of nanoneedles are observed both on top of and in between some micropillars. The main difference in growth on S17 and S19 is caused by the robustness of the photoresist that is present at the top of the micropillars, see Fig. 3. We propose that the difference in robustness is caused by the difference in exposure dose in the photolithography step. At the S17 surface the nanoneedles occasionally grow from underneath the photoresist and the photoresist is lifted off the Cu micropillar. This can be seen in Fig. 4(b). On the S19 this behavior is not observed, and as a result, the nanoneedles only grow from the sides of the micropillar.

The topography and the appearance of the structured surfaces have been investigated with the use of a Scanning Electron Microscope (SEM, FEI Apreo). The secondary electrons were detected and a beam current of 0.2 nA and an acceleration voltage of 10 kV were applied (details on SEM theory can be found in Akhtar et al. [28]).

After preparation in a clean room, the three fabricated surfaces are carefully handled in closed boxes to ensure that the structures are not damaged before the heat transfer experiments. When the substrates are attached to the Cu cylinder in the heat transfer setup, they are handled with gloves and only touched in two corners. As the width of the substrates are higher than the diameter of the cylinder, the surface at which the condensation will occur is left untouched and the surface structures are the same under the heat transfer experiments as described in this section. To confirm the stability of the structures, SEM images were recorded both before and after the condensation experiments. The results are presented in the Supplementary Information.
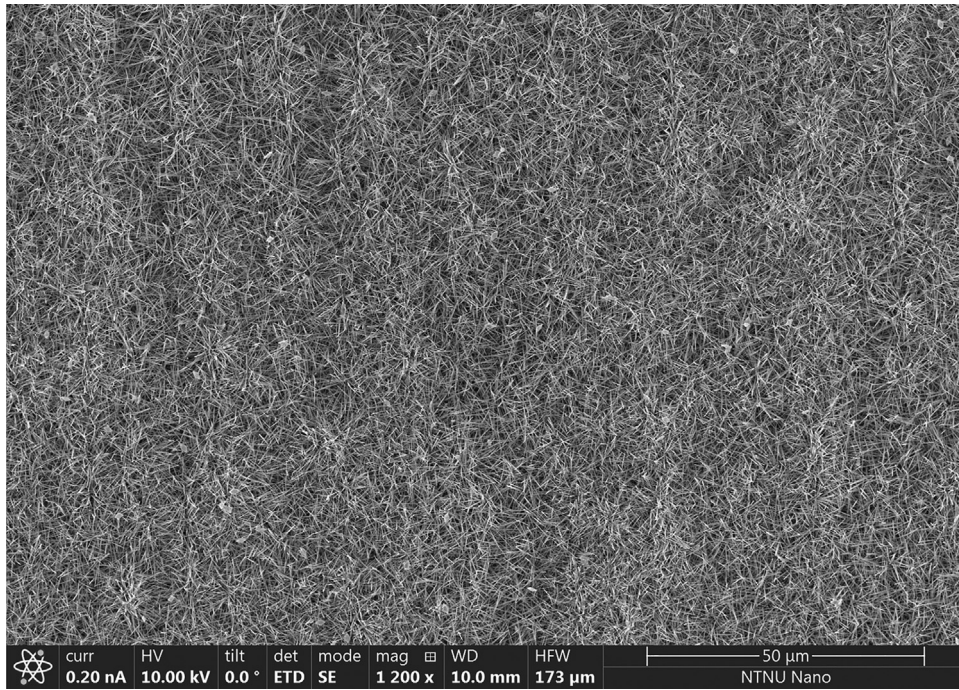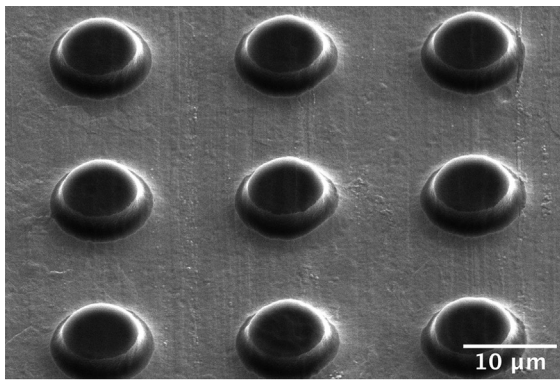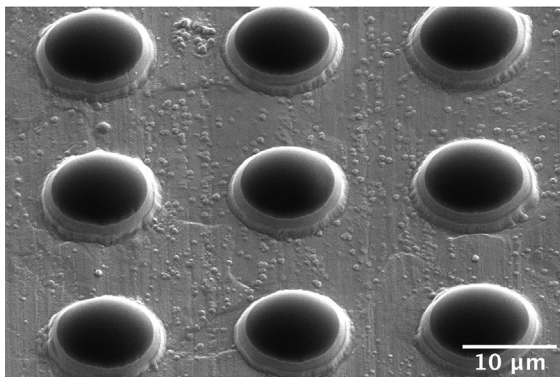
Fig. 2. Scanning Electron Microscope image of CuO nanoneedles on Cu substrate fabricated by solution immersion for 3 min. This surface is called NS.

(a)

(b)

Fig. 3. Cu surface with micropillars after deposition of photoresist and 2 times etching by CAIBE. The exposure doses in the photolithography step are (a) 1700 mJ cm^{-2} (S17) and (b) 1900 mJ cm^{-2} (S19). The micropillars' height is approximately 1 μm. The width of the base of micropillars in (a) is approx. 10 μm, and in (b) the base width is approx. 13 μm. The dark color of the surfaces of the micropillars is caused by photoresist residue. In (b) some redeposited Cu is visible between the micropillars.

2.3. Data reduction

The data acquired in the experiments are the temperatures in the four thermocouples embedded in the Cu cylinder. The heat flux and the HTCs that are presented in this work are calculated with the equations in this section.

The temperature measurements are fitted with a linear equation relating the temperatures to the location of the thermocouples within the Cu cylinder. The regression gives the temperature gradient, ∇T, through the Cu cylinder and the surface temperature of the investigated substrate, T_{surf}, by extrapolation. ∇T is used to calculate the total heat flux q_{tot} through the cylinder, according to Eq. (1), where k is the thermal conductivity of Cu.
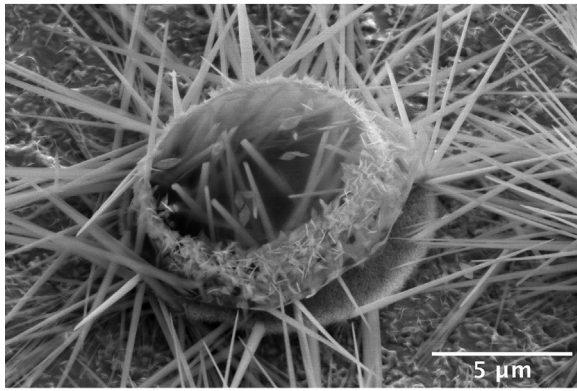
$$q_{tot} = -k\nabla T \tag{1}$$

The condensation heat flux, which is the portion of the heat flux that we are interested in, is not equal to the total heat flux through the cylinder. Some heat is transported through the insulation, some goes to cooling the gas in the pressure chamber prior to condensation, and some heat is lost internally in the investigated substrate caused by the geometrical mismatch between the spherical Cu cylinder surface and the quadratic substrates. We assume that the heat loss is independent of the subcooling of the surface versus the saturation temperature. The condensation heat flux is therefore found by linearly extrapolating the heat flux data to zero subcooling, and subtracting the resulting constant value from each data series. In this way, the condensation heat flux is zero for zero subcooling, as required. Each experiment is repeated 3-6 times. The exact number is determined by the deviation in the data from experiment to experiment. After 3 experiments we evaluated the consistency in the results and determined if another series was necessary.

The condensation HTC, h_{cond}, is defined by Eq. (2), where T_{sat} is the temperature at the given saturation pressure, T_{surf} is the surface temperature, giving the subcooling of the substrate $T_{sat} - T_{surf}$. T_{sat} is found by using the Span Wagner equation of state [29] with the pressure in the chamber as input. The NIST Webbook is used
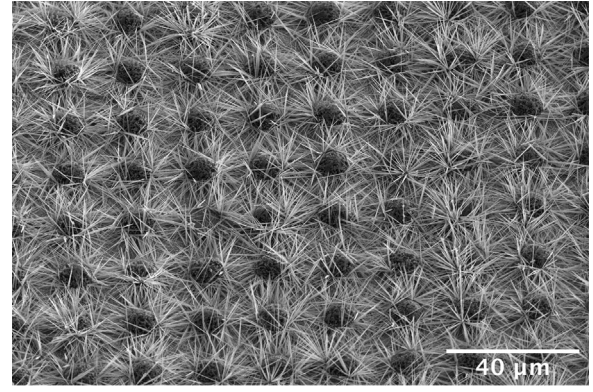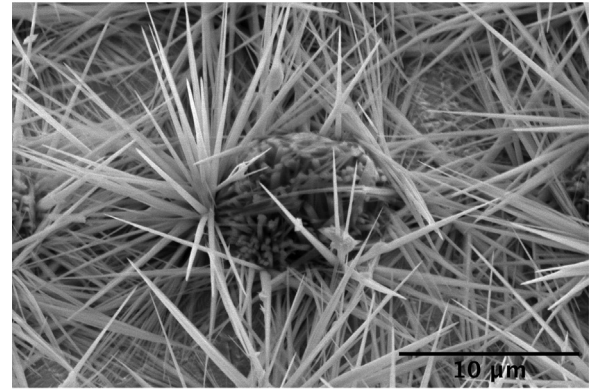
(a)

(b)

Fig. 4. SEM images of the hierarchical Cu/CuO structures for which the micro structures are fabricated with photolithography with exposure dose of 1700 mJ cm^{-2}, named S17. In (a), an overview of the surface is shown with a 1200 times magnification. In (b), one of the Cu cylinders covered in CuO flakes and nanoneedles is shown. The nanoneedles grow primarily on the top and on the sides of the microstructure, however the length of the nanoneedles are much shorter when growing on the top of the cylinder and the microscale of the Cu cylinders is intact. Smaller nanostructures, as flakes and needles, are grown at the flat surfaces between the micropillars.

Table 1
Table with the estimated uncertainties used for calculating the overall uncertainties in heat flux and subcooling.

Parameter	Uncertainty
$TC1, TC2, TC3, TC4$	±0.0337 K
P_{sat}	±0.0875 bar
T_{sat}	±0.2 K
t_{TIM}	±0.05 mm
T_{surf}	±0–0.35 K (depending on heat flux)
k_{Cu}	±0.013% [31]
$x4 - x1$	±0.04 mm

for the calculation [30].

$$h_{cond} = \frac{q_{cond}}{T_{sat} - T_{surf}} \qquad (2)$$

2.4. Uncertainty analysis

An uncertainty analysis based on the propagation of errors have been performed. The resulting expression for the total error in heat flux, E_q, is presented in Eq. (3), and the total error in subcooling is shown in Eq. (4). The values used for calculating the errors are shown in Table 1.

$$E_q = \sqrt{\left(\frac{T_4 - T_1}{d_{1-4}}\right)^2 E_k^2 + 2\left(\frac{k}{d_{1-4}}\right)^2 E_T^2 + \left(\frac{T_4 - T_1}{d_{1-4}^2}\right)^2 E_d^2} \qquad (3)$$

(a)

(b)

Fig. 5. SEM images of the hierarchical Cu/CuO structures for which the microstructures are fabricated with photolithography with exposure dose of 1900 mJ cm^{-2}, named S19. (a) shows an overview of the surface with 1200 times magnification, where the high density of nanoneedles is evident. (b) shows one of the microcylinders covered in nanoneedles, 6500 times magnification. The nanoneedles grow mainly on the sides of the cylinders and in all directions partly covering the Cu surface between the cylinders with horizontal nanoneedles.

$$E_{\Delta T} = \sqrt{E_{T_{sat}}^2 + E_{T_{surf}}^2} \qquad (4)$$

Here, E_k is the estimated error in Cu thermal conductivity, E_T is the error in the temperature measurements, and E_d is the error in the distance between the thermocouples.

The error in temperature measurements, E_T, is estimated based on the icebath calibration of the thermocouples, using the standard deviation of the estimated calibration value as a constant error in the measurements. We have estimated the temperature dependent thermal conductivity of Cu from the correlation presented by Abu-Eishah [31]. The placement of the thermocouples inside the Cu cylinder has been measured with a caliper and the error is therefore assumed to be within 0.02 mm, relating to the smallest measurable values with a caliper. The error in the saturation temperature, $E_{T_{sat}}$, is based on the given uncertainty of the pressure controller used to control the pressure in the chamber. The error in the surface temperature, $E_{T_{surf}}$, is calculated from the uncertainty in the thickness of the thermal interface material, t_{TIM}.

3. Results

Fig. 6 shows the temperature measurements in the four thermocouples embedded in the Cu cylinder during condensation experiments on the flat Cu at 15 bar. T1 is situated closest to the cylinder surface and T4 is closest to the cooling element. The tem-
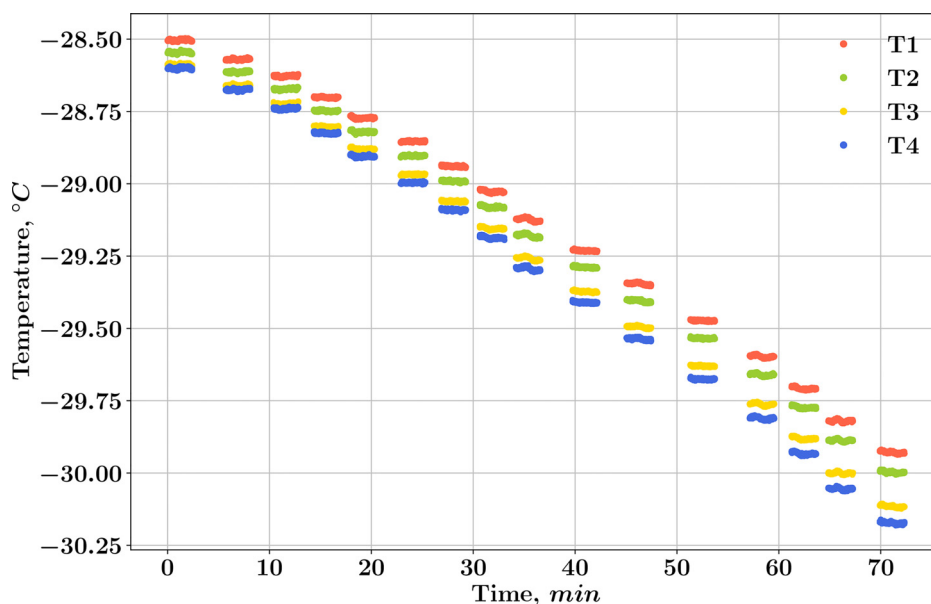
Fig. 6. Temperature measurements in the cylinder during the condensation of CO_2 on flat Cu when varying the surface temperature at 15 bar. T1–T4 are the thermocouples embedded in the cylinder, with T1 closest to the cooling element and T4 closest to the investigated surface. The jumps in time are the time it takes for a new temperature level to stabilize. Each temperature is kept for 180s.

perature gradient gradually increases with decreasing temperature in the cylinder. The jumps in time are the time it takes for a new stable temperature level to be reached. The stable temperatures are recorded for 3 min for each level of subcooling, and the resulting average temperature gradient is used to calculate the heat flux through the cylinder with Eq. (1).

The condensation heat flux of CO_2 on Cu, S17, S19, and NS as functions of subcooling are shown in Fig. 7, with chamber pressures of 10, 15, and 20 bar. For all saturation pressures, the CO_2 condensation heat flux on the S17 substrate is significantly higher than on the three other substrates. The heat flux is within the error estimate for Cu, S19 and NS, and no significant difference between the heat transfer behavior on these surfaces is observed. For all surfaces and pressures the heat flux increases with increasing subcooling between surface and saturated gas, as expected.

The condensation HTCs calculated from the heat flux data in Fig. 7 with Eq. (2), are shown in Fig. 8. For subcooling above 1K, the condensation HTC is nearly independent of subcooling on all substrates. There is a slight decrease in the condensation HTC on S17 for increasing subcooling at saturation pressures of 15 and 20 bar, while for 10 bar the HTC is approximately constant for all levels of subcooling. The condensation HTC is significantly higher on S17 compared to the other surfaces. At maximum deviation, the HTC is 66% higher on S17 than the flat Cu, S19 and NS surfaces. This occurs for 20 bar saturation pressure and approximately 1 K subcooling.

Along with the much higher values of condensation HTC on S17, the pressure dependence is also more pronounced for this surface, as shown in Fig. 9. The increase in HTC is 30% when increasing the saturation pressure from 10 to 15 bar, while it is 10% for S19, the structure with the smallest pressure dependence. When increasing the pressure from 15 to 20 bar, the HTC on Cu, S17 and S19 increases with between 1.6 and 4.2%. The HTC on the NS substrate decreases with 2.2% between 15 and 20 bar.

4. Discussion

Condensation heat transfer is a complex process and the exact physical mechanisms of the condensation on nanostructured and hierarchical structures can not be proved at this moment. Never-
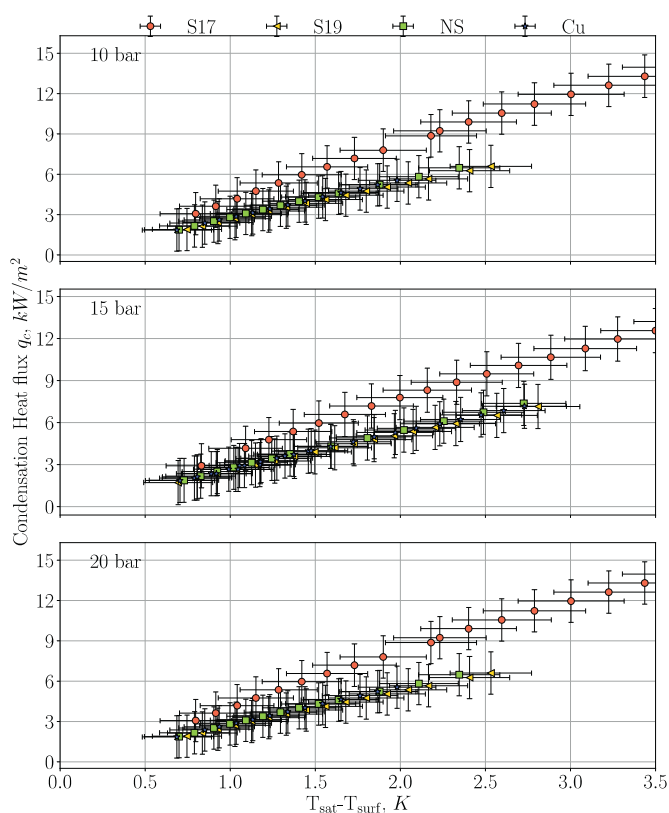

Fig. 7. Condensation heat flux data for the four investigated substrates at 10, 15, and 20 bar. Each data point is the average of repeated experiments and the errors bars are the results of the uncertainty analysis.

theless, there are results from literature that can be looked at for an indication of the heat transfer behavior on the four substrates. As seen in the results, the HTC and the heat flux on the unstructured Cu, the S19 and the NS surfaces are within the uncertainty range of each other, and therefore considered equal. This is an intriguing result, and we suggest that this is caused by three com-
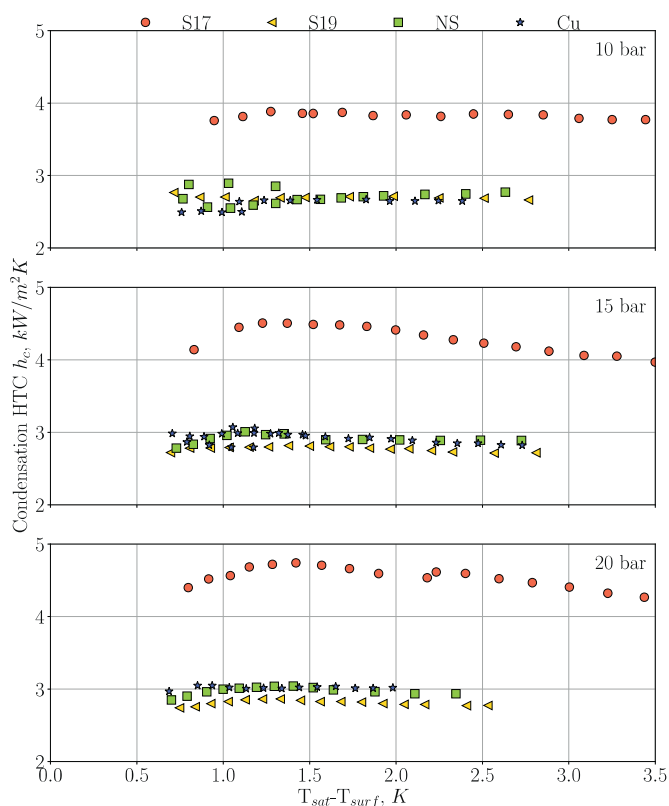
Fig. 8. Condensation HTC for Cu, S17, S19 and NS at saturation pressure of 10 bar, 15 bar, and 20 bar. Refer to Fig. 7 for uncertainty of experiments.
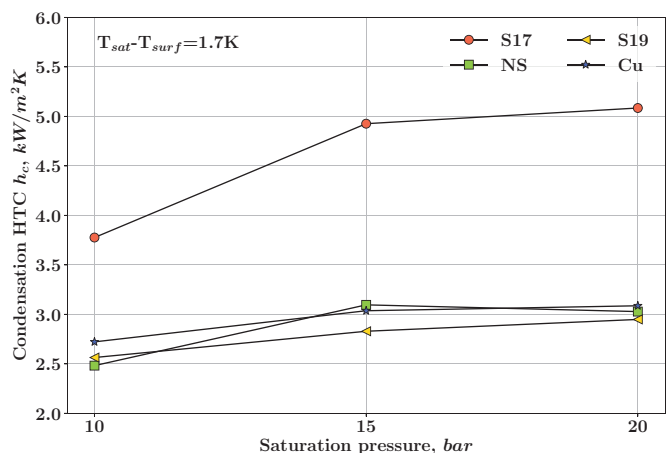

Fig. 9. The condensation HTC as a function of saturation pressure for the four investigated materials: flat Cu, S17, S19 and NS. The subcooling is 1.7 K in all cases.

Fig. 10. Sketch of the flooding of the high density nanostructured surfaces, S17 and NS.

peting effects: (1) lower thermal conductivity of CuO compared with Cu, (2) increase in surface area due to the nanostructures and (3) flooding of the nanostructures. An oxidized metallic surface generally has a lower thermal conductivity than the pure metal. This is indeed the case for Cu and CuO, for which the thermal conductivity decreases from typical values of 400 Wm^{-1} K^{-1} to 33 Wm^{-1} K^{-1} for the oxidized metal [32]. If the thermal conductivity alone would have been the determining factor, as in Hoenig et al. [33], the HTC should have been lower on the structured surfaces. It is therefore apparent that the surface structures increase the heat transfer in such a way that they balance the decrease in thermal conductivity caused by the oxidation. An increase in heat transfer due to surface structures is attributed to the increased
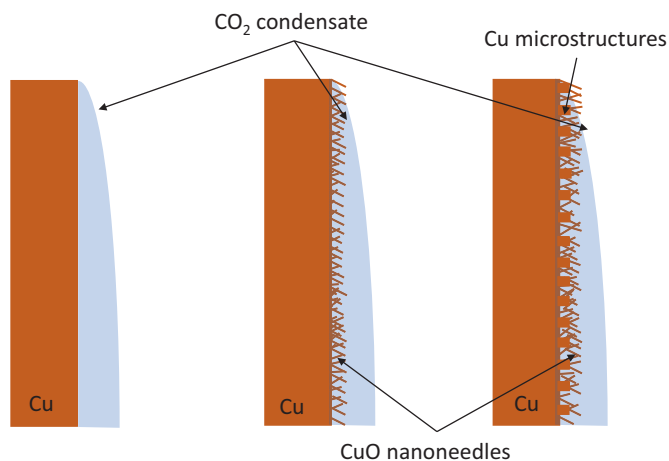
heat transfer area. This is well-known for augmented surfaces such as fins on tubes [34] and pin-fins on tubes [35]. However, if the spacing between the surface structures is small, the heat transfer increase due to augmented surface area can be counteracted by surface flooding. Ali et al. [36] showed that by lowering the spacing between the surface structures, the effect of increased heat transfer area is balanced by a heat transfer reduction caused by flooding. On both the S19 and the NS surfaces the nanoneedle density is high and the entire structures on the surfaces are therefore likely completely flooded during condensation. The resulting HTCs are within the uncertainty range of each other and indistinguishable from the HTCs on the unstructured Cu. The increase in heat transfer caused by the higher area on the surfaces are hence completely balanced by flooding and the low thermal conductivity of the CuO nanoneedles. As a consequence, the heat transfer the S19, NS and untreated Cu resembles conventional filmwise condensation on flat surfaces as elucidated in Fig. 10. The film thickness on the S19 and NS surfaces are higher than on the bare Cu surface due to liquid retention in the flooded areas, but the increase in heat transfer area balances the increased thermal resistance through the film.

The S17 surface clearly exhibits a different thermal behavior than the other surfaces. The heat flux and the HTC are significantly higher for this surface. The lower nanoneedle density increases the hierarchical nature of the surface, and reduces the likelihood of complete flooding. The surface area between the micropillars is not filled with nanoneedles, as on the S19 surface, and the flat area is beneficial for the heat transfer. The proposed condensation mechanism is that the nucleation and spreading of the condensate film occurs on the non-structured areas between the micropillars and that the nanoneedles and the micropillars reduce the film thickness. The unstructured areas between the micropillars are not completely flat, and spikes and grooves are available nucleation sites. The reduced film thickness is a result of a more efficient drainage of the CO$_2$ liquid along the space between the micro- and nanostructures, compared to the pinned liquid on the S19 and NS surfaces. Efficient drainage will lead to a thinner CO$_2$ liquid film, which again increases the HTC.

According to the model by Ali et al. [36], flooding is less likely to occur on the S17 surface due to the larger spacing between the structures. Returning to the effect of the three competing factors 1), 2) and 3) above, where the latter was related to flooding, the resulting the HTC is higher on S17 compared to S19 and NS. In contrast to the work by Aili et al. [19], we here show that an optimal combination of micro- and nanostructures is beneficial for

heat transport in certain cases, and especially when the hierarchical nature of the surface is pronounced, such as for S17.

The influence of pressure on the heat transfer is highest for the NS and the S17 surface, which both show a high increase in the HTC between 10 and 15 bar, see Fig. 9. The S17 surface also exhibit a slight increase in HTC when reaching 20 bar saturation pressure, while the HTC on the NS structure decreases between 15 and 20 bar saturation pressure. According to Preston et al. flooding of the nanostructures will occur in wicking condensation at high values of subcooling due to the high amount of condensate as the subcooling is increased [37]. When increasing the saturation pressure, on the other hand, the condensate film thickness decreases and the HTC increases. Flooding is therefore not the likely explanation of the apparent saturation of the HTC. The plateau in the HTC is therefore explained by the fluid properties of CO_2 and how these are altered with pressure. Especially, the viscosity is decreased with increasing pressure and the result could be a higher downward flow rate of the liquid. This would again lead to a thinner liquid film and an increased heat transfer. One could imagine that the liquid flow down the surface deteriorates the nanostructures, and that this could influence the pressure dependence of the heat transfer. The nanoneedles could be bent or broken and flushed down along with the condensate. We have, however, investigated the surfaces before and after condensation, and find that both the micropillars and nanoneedles are intact after repeated condensation experiments. Details can be found in Supplementary Information.

5. Conclusions and outlook

We have in this work experimentally investigated the heat transfer behavior of Cu based surfaces during the condensation of CO_2. Three different micro- and nanostructured surfaces have been fabricated and compared in terms of heat flux and heat transfer coefficient during the condensation. The surfaces are (1) a purely nanostructured surface where CuO nanoneedles are grown on a Cu substrate, (2) a hierarchical surface with Cu micropillars underneath CuO nanoneedles with high density, and (3) a surface similar to the second, but where the nanoneedles are much less dense. We have shown that when the right balance between structured and unstructured surface area is found, the outcome is an increase in the condensation heat transfer. On surfaces with a high density of CuO nanoneedles, the reduced heat transfer due to lower thermal conductivity of the oxidized surface and increased heat transfer due to the higher effective surface area neutralize each other. The HTCs are therefore similar on the purely nanostructured surface, the micro- and nanostructured surface with high nanostructure density, and the flat untreated surface. However, when the density of the nanostructures is lower, such that the true hierarchical nature of the surface is more pronounced, the HTC is increased with maximum 66% compared to the untreated surface. The work show that surface structures have a potential of increasing condensation heat transfer of CO_2 if designed and fabricated properly. The optimal design criteria have yet to be developed, but the path of hierarchical surfaces is very promising and should be followed in future work.

Declaration of Competing Interest

Authors declare that they have no conflict of interest.

CRediT authorship contribution statement

Ingrid Snustad: Conceptualization, Methodology, Software, Validation, Formal analysis, Investigation, Data curation, Writing - original draft, Writing - review & editing, Visualization. **Lene Hollund:** Validation, Investigation, Data curation, Writing - review & editing. **Åsmund Ervik:** Conceptualization, Methodology, Software, Validation, Formal analysis, Writing - review & editing, Supervision. **Anders Austegard:** Methodology, Formal analysis, Writing - review & editing. **Amy Brunsvold:** Conceptualization, Methodology, Writing - review & editing, Supervision. **Jianying He:** Writing - review & editing, Supervision. **Zhiliang Zhang:** Conceptualization, Methodology, Formal analysis, Writing - review & editing.

Supplementary material

Supplementary material associated with this article can be found, in the online version, at 10.1016/j.ijheatmasstransfer.2021.121367

References

[1] S.K. Fischer, Total equivalent warming impact: a measure of the global warming impact of CFC alternatives in refrigerating equipment, Int. J. Refrig. 16 (6) (1993) 423–428, doi:10.1016/0140-7007(93)90059-h.

[2] K.M. Tsamos, Y.T. Ge, I. Santosa, S.A. Tassou, G. Bianchi, Z. Mylona, Energy analysis of alternative CO_2 refrigeration system configurations for retail food applications in moderate and warm climates, Energy Convers. Manag. 150 (2017) 822–829, doi:10.1016/j.enconman.2017.03.020.

[3] S. Liu, H. Qi, V. Nian, B. Liu, B. Dai, Z. Sun, X. Li, J. Yuan, A new correlation for carbon dioxide boiling heat transfer coefficient outside evaporating tubes, J. Clean. Prod. 276 (2020) 123050, doi:10.1016/j.jclepro.2020.123050.

[4] B. Dai, H. Qi, S. Liu, M. Ma, Z. Zhong, H. Li, M. Song, Z. Sun, Evaluation of transcritical CO_2 heat pump system integrated with mechanical subcooling by utilizing energy, exergy and economic methodologies for residential heating, Energy Convers. Manag. 192 (2019) 202–220, doi:10.1016/j.enconman.2019.03.094.

[5] A. Aspelund, K. Jordal, Gas conditioning - the interface between CO_2 capture and transport, Int. J. Greenhouse Gas Control 1 (3) (2007) 343–354, doi:10.1016/s1750-5836(07)00040-0.

[6] F. Neele, R. de Kler, M. Nienoord, P. Brownsort, J. Koornneef, S. Belfroid, L. Peters, A. vanWijhe, D. Loeve, CO_2 transport by ship: the way forward in Europe, in: 13th International Conference on Greenhouse Gas Control Technologies, GHGT-13, 114, Energy Procedia, 2017, pp. 6824–6834, doi:10.1016/j.egypro.2017.03.1813.

[7] E.S. Rubin, J.E. Davison, H.J. Herzog, The cost of CO_2 capture and storage, Int. J. Greenhouse Gas Control 40 (2015) 378–400, doi:10.1016/j.ijggc.2015.05.018.

[8] I. Snustad, I.T. Røe, A. Brunsvold, Å. Ervik, J. He, Z. Zhang, A review on wetting and water condensation - perspectives for CO_2 condensation, Adv. Colloid Interface Sci. 256 (2018) 291–304, doi:10.1016/j.cis.2018.03.008.

[9] D. Attinger, C. Frankiewicz, A.R. Betz, T.M. Schutzius, R. Ganguly, A. Das, C.-J. Kim, C.M. Megaridis, Surface engineering for phase change heat transfer: a review, MRS Energy Sustain. 1 (2014), doi:10.1557/mre.2014.9.

[10] T.J. Hendricks, S. Krishnan, C. Choi, C.-H. Chang, B. Paul, Enhancement of pool-boiling heat transfer using nanostructured surfaces on aluminum and copper, Int. J. Heat Mass Transf. 53 (15-16) (2010) 3357–3365, doi:10.1016/j.ijheatmasstransfer.2010.02.025.

[11] Y. Nam, S. Sharratt, G. Cha, Y.S. Ju, Characterization and modeling of the heat transfer performance of nanostructured Cu micropost wicks, J. Heat Transf. 133 (10) (2011) 101502, doi:10.1115/1.4004168.

[12] D. Saeidi, A.A. Alemrajabi, Experimental investigation of pool boiling heat transfer and critical heat flux of nanostructured surfaces, Int. J. Heat Mass Transf. 60 (2013) 440–449, doi:10.1016/j.ijheatmasstransfer.2013.01.016.

[13] C. Li, Z. Wang, P.-I. Wang, Y. Peles, N. Koratkar, G.P. Peterson, Nanostructured copper interfaces for enhanced boiling, Small 4 (8) (2008) 1084–1088, doi:10.1002/smll.200700991.

[14] R. Chen, M.-C. Lu, V. Srinivasan, Z. Wang, H.H. Cho, A. Majumdar, Nanowires for enhanced boiling heat transfer, Nano Lett. 9 (2) (2009) 548–553, doi:10.1021/nl8026857.

[15] J.B. Boreyko, C.-H. Chen, Self-propelled dropwise condensate on superhydrophobic surfaces, Phys. Rev. Lett. 103 (18) (2009), doi:10.1103/PhysRevLett.103.184501.

[16] J. Cheng, A. Vandadi, C.-L. Chen, Condensation heat transfer on two-tier superhydrophobic surfaces, Appl. Phys. Lett. 101 (13) (2012) 131909, doi:10.1063/1.4756800.

[17] R. Wen, X. Ma, Y.-C. Lee, R. Yang, Liquid-vapor phase-change heat transfer on functionalized nanowired surfaces and beyond, Joule 2 (11) (2018) 2307–2347, doi:10.1016/j.joule.2018.08.014.

[18] J. Ma, S. Sett, H. Cha, X. Yan, N. Miljkovic, Recent developments, challenges, and pathways to stable dropwise condensation: a perspective, Appl. Phys. Lett. 116 (26) (2020) 260501, doi:10.1063/5.0011642.

[19] A. Aili, Q. Ge, T. Zhang, Effect of Mini/Micro/Nanostructures on Film-wise Condensation of Low-Surface-Tension Fluids, J. Heat Transf. 140 (10) (2018) 102402, doi:10.1115/1.4040143. https://asmedigitalcollection.asme.org/heattransfer/article-pdf/140/10/102402/6219575/ht_140_10_102402.pdf

[20] H.M. Ali, An analytical model for prediction of condensate flooding on horizontal pin-fin tubes, Int. J. Heat Mass Transf. 106 (2017) 1120–1124, doi:10.1016/j.ijheatmasstransfer.2016.10.088.

[21] H.M. Ali, A. Briggs, A semi-empirical model for free-convection condensation on horizontal pin-fin tubes, Int. J. Heat Mass Transf. 81 (2015) 157–166, doi:10.1016/j.ijheatmasstransfer.2014.10.008.

[22] A.T. Wijayanta, T. Miyazaki, S. Koyama, Refrigerant distribution in horizontal headers with downward minichannel-branching conduits: experiment, empirical correlation and two-phase flow pattern map, Exp. Therm. Fluid Sci. 81 (2017) 430–444, doi:10.1016/j.expthermflusci.2016.09.011.

[23] J. Wu, Å. Ervik, I. Snustad, S. Xiao, A. Brunsvold, J. He, Z. Zhang, Contact angle and condensation of a CO_2 droplet on a solid surface, J. Phys. Chem. C 123 (1) (2019) 443–451, doi:10.1021/acs.jpcc.8b08927.

[24] J. Wu, I. Snustad, Å. Ervik, A. Brunsvold, J. He, Z. Zhang, CO_2 wetting on pillar-nanostructured substrates, Nanotechnology 31 (24) (2020) 245403, doi:10.1088/1361-6528/ab7c49.

[25] I. Snustad, Å. Ervik, A. Austegard, A. Brunsvold, J. He, Z. Zhang, Heat transfer characteristics of CO_2 condensation on common heat exchanger materials: method development and experimental results, 2021. Under Review.

[26] Z. He, J. He, Z. Zhang, Selective growth of metallic nanostructures on microstructured copper substrate in solution, CrystEngComm 17 (2015) 7262–7269, doi:10.1039/C5CE01093D.

[27] Z. He, Z. Zhang, J. He, CuO/Cu based superhydrophobic and self-cleaning surfaces, Scr. Mater. 118 (2016) 60–64, doi:10.1016/j.scriptamat.2016.03.015. http://www.sciencedirect.com/science/article/pii/S1359646216300884

[28] K. Akhtar, S.A. Khan, S.B. Khan, A.M. Asiri, Scanning electron microscopy: principle and applications in nanomaterials characterization, in: Handbook of Materials Characterization, Springer International Publishing, 2018, pp. 113–145, doi:10.1007/978-3-319-92955-2_4.

[29] R. Span, W. Wagner, A new equation of state for carbon dioxide covering the fluid region from the triple-point temperature to 1100 K at pressures up to 800 MPa, J. Phys. Chem. Ref. Data 25 (6) (1996) 1509–1596, doi:10.1063/1.555991.

[30] National Institute of Standards and Technology, 2018, https://webbook.nist.gov/chemistry/fluid/.

[31] S.I. Abu-Eishah, Correlations for the thermal conductivity of metals as a function of temperature, Int. J. Thermophys. 22 (6) (2001) 1855–1868, doi:10.1023/a:1013155404019.

[32] M. Liu, M. Lin, C. Wang, Enhancements of thermal conductivities with Cu, CuO, and carbon nanotube nanofluids and application of MWNT/water nanofluid on a water chiller system, Nanoscale Res. Lett. 6 (1) (2011) 297, doi:10.1186/1556-276x-6-297.

[33] S.H. Hoenig, S. Modak, Z. Chen, M. Kaviany, J.F. Gilchrist, R.W. Bonner, Role of substrate thermal conductivity and vapor pressure in dropwise condensation, Appl. Therm. Eng. 178 (2020) 115529, doi:10.1016/j.applthermaleng.2020.115529.

[34] C.-Y. Zhao, W.-T. Ji, P.-H. Jin, Y.-J. Zhong, W.-Q. Tao, The influence of surface structure and thermal conductivity of the tube on the condensation heat transfer of R134A and R404A over single horizontal enhanced tubes, Appl. Therm. Eng. 125 (2017) 1114–1122, doi:10.1016/j.applthermaleng.2017.06.133.

[35] H.M. Ali, A. Briggs, Condensation of ethylene glycol on pin-fin tubes: effect of circumferential pin spacing and thickness, Appl. Therm. Eng. 49 (2012) 9–13, doi:10.1016/j.applthermaleng.2011.08.017.

[36] H.M. Ali, M.Z. Qasim, M. Ali, Free convection condensation heat transfer of steam on horizontal square wire wrapped tubes, Int. J. Heat Mass Transf. 98 (2016) 350–358, doi:10.1016/j.ijheatmasstransfer.2016.03.053.

[37] D.J. Preston, K.L. Wilke, Z. Lu, S.S. Cruz, Y. Zhao, L.L. Becerra, E.N. Wang, Gravitationally driven wicking for enhanced condensation heat transfer, Langmuir 34 (15) (2018) 4658–4664, doi:10.1021/acs.langmuir.7b04203.